The effect of sinusoidal fins' amplitude on the thermo-hydraulic performance of a solar air heater

Zoheir Saboohi[a,*], Fathollah Ommi[a,b], Ebrahim Rahmani[c], Tofigh Moradi[c], Abolfazl Fattahi[d], Mostafa Delpisheh[c], Nader Karimi[e,f]

[a] *A & S Institute, Ministry of Science, Research, and Technology, Tehran, Iran*
[b] *Department of Mechanical Engineering, Tarbiat Modares University, Tehran, Iran*
[c] *School of Mechanical Engineering, Iran University of Science and Technology, Tehran, Iran*
[d] *Department of Mechanical Engineering, University of Kashan, Kashan, Iran*
[e] *School of Engineering, University of Glasgow, Glasgow G12 8QQ, United Kingdom*
[f] *School of Engineering and Materials Science, Queen Mary University of London, London E1 4NS, United Kingdom*

Corresponding author:* Zoheir Saboohi, Assistant Professor, zoheir.saboohi@gmail.com

The effect of sinusoidal fins' amplitude on the thermo-hydraulic performance of a solar air heater

Abstract

Solar energy exploitation is growing consistently, as it is the cheapest and most accessible amongst all forms of renewable energies. Increasing the performance of solar air heaters can aid in developing clean energy use and subsiding the greenhouse gas emissions from in the world. This study, therefore, seeks to improve the thermo-hydraulic performance of solar air heaters using sinusoidal extended surfaces. The results show that Reynolds number increment contributes to the enhancement of Nusselt number and thermo-hydraulic performance, while it does not affect the friction factor considerably. The highest value of the Nusselt number belongs to the case with the highest fin amplitude and wavy fins configuration by about 7 times higher value in comparison to the simple solar air heater. It is shown that the wavy configuration can render higher thermo-hydraulic performance than that of raccoon fins, by about 10 percent. The finned configurations feature better fluid flow mixing at the outlet and lower maximum and gradient of temperature on the absorber plate compared to those of simple and common solar air heaters.

Keywords: solar air heater; wavy and raccoon fin; numerical simulation; thermal performance factor.

Nomenclature

A	Amplitude	**Greek letters**	
A_P	Absorber area	α	Thermal diffusivity

C_p	Thermal capacity	Δp	Pressure drop
D_h	Hydraulic diameter (m)	ε	Turbulence dissipation rate
E_{ij}	Rate of deformation	λ	Length period
f	Friction factor	μ	Dynamic viscosity
h	Heat transfer coefficient	μ_t	Eddy viscosity
k	Turbulence kinetic energy (J/kg)	υ	Kinematic viscosity
K	Thermal conductivity	ρ	Density
L	Length of SAH	∞	Far field
$\dot{m}$	Mass flow rate		
Nu	Nusselt number	**Subscripts**	
p	Pressure	i	Inlet
Pr	Prandtl number	o	Outlet
$\dot{Q}$	Thermal power	s	Simple SAH (without fins)
Re	Reynolds number	avg	Average
T	Temperature		
T_a	Average temperature of absorber	**Abbreviation**	
T_{avg}	Average temperature of the flow	SAH	Solar air heater
u_i	Velocity	THPP	Thermo-hydraulic performance parameter
V_m^2	Average velocity (or bulk velocity)	THEF	Thermo-hydraulic enhancement factor
W	Distance between two fins	TKE	Turbulent kinetic energy

1. Introduction

A solar air heater (SAH) is a cheap device, which captures different wavelengths of solar irradiation and converts it into useful thermal energy (Yadav and Bhagoria 2013a; Gawande et al. 2016). By heating air, this renewable energy is applicable for moderate and low-temperature applications, such as direct solar drying (Raj et al. 2019; ElGamal et al. 2020 Nov), dehydration of food (Madhlopa et al. 2002), residential heating (Paraschiv et al. 2020; Singh et al. 2020; Treichel and Cruickshank 2021), etc. In some applications, SAH is more suitable in comparison with liquid collectors, due to eliminating heat transfer between one fluid and another (Arul Kumar et al. 2016; Arunkumar et al. 2020). Inside the SAH, a laminar viscous layer is formed through airflow that is attached to the absorbing plate, resisting the exchange of thermal energy between the plate and airflow in contact (Yadav and Bhagoria 2013b; Boulemtafes-Boukadoum and

Benzaoui 2014). The heat transfer coefficient is low grounded concerning the absorber plate and the airflow in contact, and roots in poor efficiency. The performance of SAH hinges on parameters, such as the intensity of solar irradiation, convection among absorber and air, absorber plate losses, etc. Scientists have concentrated on these parameters and correspondingly amended the design of SAHs to improve their performance. One of the efficient remedies for strengthening the convection in the SAH is using fins in various shapes, such as simple, sinusoidal, or helical geometry. This has been considered in the literature, as reviewed in the following.

Singh and Singh (2018) studied the thermal performance of a roughened square wave profiled transverse ribbed SAH, using the RNG k-ε turbulence model, validated by experimental investigations. The Nusselt number and friction factor over a smooth duct was reported to be improved 2.14 and 3.55 times, respectively. Thermo-hydraulic performance parameter was observed to be 1.43. At a 10 relative pitch roughness and Reynolds number of 12,000, the thermo-hydraulic performance parameter experienced a 1.43 maximum. In an experiment by Priyam and Chand (2019), fin spacing, mass flow rate, and insolation of wavy finned SAH were studied; it was witnessed to be 67.44 to 121.43% thermally efficient for 0.00312–0.0158 kg/s mass flow rate and 2–6 cm fin spacing. It was observed that the absorber plate encompassing corrugated fins had maximum efficiency at minimum cost through evaluating different configurations of absorber plates. Issacci et al. (1988) developed a theoretical model for performance evaluation of finned SAHs and carried out a parametric study. They reported that through lower fin surface emissivity and conductivity (thin fins), the efficiency of the SAH increases.

Kasperski and Nemś (2013) investigated the thermo-hydraulic characteristics of different internal-fin array configurations in SAHs by proposing a heat transfer mathematical model. The geometry allows a reduction in airflow demanded, 7-10 fold, and at the same time gains a higher

efficiency, in comparison to smooth pipe absorber arrangement. Madhu et al. (2020) coated the absorber of SAH with CNT-black paint and also introduced staggered fins. The coating effect enhanced the plate temperature from 95 °C to a maximum of 102 °C and the average daily efficiency improved by up to 98% at lower mass flow rates. A numerical study was presented by Naphon (2005) on double-pass flat plate SAH, fitted with longitudinal fins at 0.02 and 0.1 kg/s mass flow rates to predict entropy generation and height and number of fin effects. It was addressed that through an increase in height and number of fins, the thermal efficiency increases, and entropy generation decreases.

Sahu et al. (2019) reviewed the application of extended surfaces, namely longitudinal fins, to enhance the thermal performance of SAHs; they asserted that the increase of fin height, number of glass covers, and the decrease of duct depth will lead to higher performances. Meanwhile, the literature indicated that the friction factor behaves contrariwise to mass flow rate, while the Nusselt number increases, correspondingly. Kannan et al. (2020) experimentally investigated embedding pin-fins in a solar air heater with jet impingement. The maximum improvement of 12 % in energy efficiency, along with the advancement of exergy efficiency and air outlet temperature was also reported. Similar experiments were conducted by Sivakumar et al. (2019). Despite considerable thermal enhancement declared, the pressure drop could increase about 60 % in comparison to a flat absorber without fins. Generalized predictor correlations were presented by Kumar et al. (2020) for a curved-ribbed solar air heater with reasonable precision. Similar correlations were derived by Kumar et al. (2019) for a solar air heater equipped with multiple-arc shaped ribs. Despite the significant thermal achievement, the pressure drop took high values. Singh et al. (2014) examined the artificial roughness in a similar configuration (Singh et al. 2014b; Kumar et al. 2019). They found that the thermo-hydraulic performance and the roughness did not have a linear

relationship. The effects of Reynolds number, rib-pitch, rib-height, number of gaps, arc-attack angle, rib, and gap width on the thermo-hydrodynamic performance of a solar air heater having roughened multiple-arc-rib patterns were examined by Kumar et al. (2021). An increment of 5.7 and 6 folds were reported for Nusselt number and friction factor, respectively, compared to a smooth solar heater. They added that the aiding contribution of the Nusselt number can overcome the negative effects of the friction factor, as the thermo-hydraulic performance touched the value of 3.4, also qualitatively supported by (Kumar, Goel, et al. 2020).

An experiment was put through by Skullong et al. (2016) on heat transfer and energy loss caused by friction in an innovative SAH inaugurated with wavy-groove and wing vortex generators. This combination resulted in a 37.7-46.3% increase in thermal performance and yielded a 2.24 thermal enhancement factor while increasing Nusselt number and friction factor. Wavy-finned SAH was analytically explored by Priyam and Chand (2016) and an expression was proposed for collector efficiency. It was observed that thermal efficiency and effective temperature rise of wavy-finned SAH were 62.53 % and 63.41%, through the lowest fin spacing. An experimental investigation was presented by Priyam and Chand (2018) on wavy-finned SAH, evaluating spacing of fins, mass flow rate parameters to appraise the heat transfer performance. They reported that through a 2 cm fin spacing, thermal efficiency experienced a 116.67% increase. Also, compared to 6 cm spacing, it was 28.71% higher. In another study, Priyam and Chand (2017) evaluated the pressure drop and heat transfer, considering flow rate and collector length. They addressed that for mass flow rates less than 0.05 kg/s, by increasing the length, the valuable energy gain and pressure drop rises as well, nevertheless, reducing the efficiency. They added that the length would be ineffective at higher mass flow rates.

Kumar and Chand (2017) assessed herringbone corrugated fins application in SAH. This amendment was observed to give improved thermal and thermo-hydraulic efficiency compared to plane SAH, addressing that the thermal efficiency experienced a 36.2% increase and the thermo-hydraulic efficiency experienced a 56.6%; this occurred at a fin pitch of 2.5 cm and 0.026 kg/s mass flow rate. Furthermore, thinning the gap between the corrugated fins and increasing the mass flow rate, increased the pressure drop. In a SAH encompassing inclined fins, Nusselt number, friction factor, and thermohydraulic performance factor were scrutinized by Qader et al. (2019). They specified that a momentous heat transfer enhancement was achieved by this adjustment. Moreover, the thermo-hydraulic performance factor was addressed at 1.916, the literature comparison: square (1.80), L-shaped (1.90), and circle (1.65).

Several works have been devoted to fins application in SAHs, as the preceding review shows. Nonetheless, the sinusoidal fin shapes are applied more limitedly. Owing to the successful use of this type of fins in heat exchangers (Sadeghianjahromi and Wang 2020 Oct; Hu and Li 2021; Sertkaya and Sari 2021), this study aims to involve the benefits of sinusoidal fins in SAH. Two configurations of wavy and raccoon are examined through a numerical simulation. The effect of Reynolds number and fins' amplitude, showing the deviations of the flow paths on the plate, on the thermo-hydraulic performance of the SAH is assessed.

2. Solution details

2.1. Governing equations

The governing equations are the cornerstone of computational fluid dynamics, which mathematize the physics of fluids. In the computational domain, considering a steady-state, 3D,

Newtonian, incompressible and devoid of viscous dissipation for the airflow, the governing equations for continuity, momentum, and energy are as follows (Yadav and Saini 2020):

$$\frac{\partial(\rho u_i)}{\partial x_i} = 0 \tag{1}$$

$$\frac{\partial}{\partial x_i}(\rho u_i u_i) = -\frac{\partial p}{\partial x_i} + \frac{\partial}{\partial x_j}\left[\mu\left(\frac{\partial(\rho u_i)}{\partial x_i} + \frac{\partial(\rho u_i)}{\partial x_i}\right)\right] + \frac{\partial}{\partial x_i}(-\overline{\rho u_i u_i}) \tag{2}$$

$$\frac{\partial}{\partial x_i}(\rho u_i T) = \frac{\partial}{\partial x_j}\left(\frac{\lambda}{C_p}\frac{\partial T}{\partial x_j}\right) \tag{3}$$

Herein ρ, u_i, p, and T denote density, velocity, pressure, and temperature, respectively. Also, μ, λ, and C_p correspondingly allude to dynamic viscosity, thermal conductivity, and thermal capacity. Moreover, in the solid regions of fins, the conduction heat transfer is solved.

Choosing a suitable turbulence model is crucial in reducing the simulation time and also the errors entailed during modeling. The RNG $k-\varepsilon$ is nominated in this study as the turbulence model, due to its high ability for capturing the physics of flows comprising potential separation and secondary flows (Speziale and Thangam 1992). It has also been recommended by comparing various turbulence models in the literature following similar numerical simulations (Xue et al. 2018). The corresponding transport equations are as follows (Yakhot et al. 1992):

$$\frac{\partial(\rho k)}{\partial t} + \frac{\partial(\rho k u_i)}{\partial x_i} = \frac{\partial}{\partial x_j}\left[\frac{\mu_t}{\sigma_k}\left(\frac{\partial k}{\partial x_j}\right)\right] + 2\mu_t E_{ij}E_{ij} - \rho\varepsilon \tag{4}$$

$$\frac{\partial(\rho\varepsilon)}{\partial t} + \frac{\partial(\rho\varepsilon u_i)}{\partial x_i} = \frac{\partial}{\partial x_j}\left[\frac{\mu_t}{\sigma_\varepsilon}\left(\frac{\partial \varepsilon}{\partial x_j}\right)\right] + C_{1\varepsilon}\frac{\varepsilon}{k}2\mu_t E_{ij}E_{ij} - C_{2\varepsilon}\rho\frac{\varepsilon^2}{k} \tag{5}$$

$$\mu_t = \rho C_\mu \frac{k^2}{\varepsilon} \tag{6}$$

where k, μ_t, and ε, indicate the turbulence kinetic energy, eddy viscosity, and turbulence dissipation rate, individually. The constants involved are defined as $\sigma_k = 1.00$, $\sigma_\varepsilon = 1.30$, $C_{1\varepsilon} =$

1.44, and $C_{2\varepsilon} = 1.92$ (Szablewski 1973). The enhanced wall treatment was also used along with the turbulence model.

In evaluating the thermal performance, the average Nusselt number is the main central parameter in this problem, written as:

$$Nu = \frac{hD_h}{k} \tag{7}$$

where h and D_h are heat transfer coefficient and hydraulic diameter, derived through:

$$h = \frac{\dot{Q}}{A_P(T_a - T_{avg})} \tag{8}$$

in which $\dot{Q}$ is thermal power, A_P the absorber area, T_a is the average temperature of the absorber, calculated using area-weighted average and T_{avg} is the average temperature of the flow, determined through the arithmetic average of the temperature of fluid flow at the inlet and outlet ($T_{avg} = \frac{T_i + T_o}{2}$). The thermal power is calculable through:

$$\dot{Q} = \dot{m}C_p(T_o - T_i) \tag{9}$$

In Eq. (9), T_o and T_i denote inlet and outlet flow temperature. For the fluid flow in the SAH, the friction factor is implemented for hydraulic assessment, determined through (Skullong et al. 2018; Qader et al. 2019):

$$f = \frac{(\Delta P)D_h}{2\rho L V_m^2} \tag{10}$$

ΔP and D_h respectively show the pressure drop and hydraulic diameter. Also, L and V_m^2 denote the length of SAH and the bulk velocity. The thermal performance factor (THPF) is the thermo-hydraulic evaluation, which is defined as (Kumar et al. 2017; Singh 2020):

$$THPF = \frac{(Nu/Nu_s)}{(f/f_s)^{1/3}} \quad (11)$$

is the most prominent parameter for appraising the performance overall. The subscript s defines the simple SAH without fins in Eq. (11).

2.2. Boundary conditions, fluid flow properties, and solving procedure

Herein, the boundary conditions applied for the current problem are defined. The solid walls of the SAH under analysis, comprising the boundary walls and fins, are hydrodynamically regarded as no-slip conditions. The fins are considered to be thermally coupled with the fluid flow field, while the other walls are considered adiabatic. The absorber plate, however, is heated through a $900\mathrm{W/m^2}$ solar flux. A constant velocity is set for the fluid flow at the inlet, defined using the Reynolds number, and $300\mathrm{K}$ temperature. The outlet condition, on the other hand, is defined by known gauge pressure of zero.

Owing to temperature variations in the domain, the air thermo-physical properties are defined as being functions of temperature. Subsequently, the mentioned parameters are demonstrated through (Antony et al. 2020):

$$\rho = 3.9147 - 0.016082T + 2.9013 \times 10^{-5}T^2 - 1.9407 \times 10^{-8}T^3 \quad (12)$$

$$\mu = (1.6157 + 0.06523T - 3.0297 \times 10^{-5}T^2 - 1.9407) \times 10^{-6} \quad (13)$$

$$k = (0.0015215 + 0.09746T - 0.3322 \times 10^{-5}T^2) \times 10^{-3} \quad (14)$$

The finite volume method is implemented for solving the governing equations, utilizing the pressure-based solver. The second-order upwind scheme is used for the discretization of transport equations. Green-Gauss node based is applied for the spatial gradient discretization. The semi-implicit method for pressure-linked equations, commonly abbreviated as SIMPLE, is put through

for pressure-velocity coupling. The convergence criteria are considered as the residual sums of less than 10^{-5} for the governing equations.

2.3. Geometries studied

The SAH is comprised of a simple cubic duct, whereby the upper wall is the absorber, which collects the thermal flux irradiation. Wavy and raccoon-shaped fins are inaugurated on the absorber plate's inner side. **Figure 1a** illustrates the schematics of the configurations with millimeter dimensions. Moreover, the details of the mentioned longitudinal wavy and raccoon-shaped fins are depicted in **Figure 1b** and **Figure 1c**, respectively.

As observed in **Figure 1**, the wavy and raccoon-shaped fins are identified via the relative arrangement of the sinusoidal fins to each other. The fin's geometry is delineated by the amplitude, A, the length period, λ, and spatial distance between two successive fins, W, as presented in **Figure 2**. In this study, the following values are considered, $\lambda = 45\text{mm}$, $A = 3.78$ or 7.50mm, and $W = 20\text{mm}$.

The geometrical characteristics, namely, the height of the fins and the SAH configuration are different in the cases studied, charted in **Table 1**. The cases studied varies in terms of fins configuration, named wavy and raccoon, and amplitude values.

2.4. Solution validation, meshing, and grid independency test

Since a similar study on the SAH is infrequent, the validation step is primarily executed through the comparison of the average Nusselt number of a turbulent channel flow on a hot surface, between the upshots of the present study and the results reported by Dittus-Boelter correlation (Theodore L. Bergman 2011). Moreover, a study by Kumar and Layek (2019) is also considered for validation, which experimented the twisted ribs attached to the hot plate in a simple SAH

arrangement. The thermal comparison is depicted in **Figure 3a**, illustrating an average of 5 % disparity. Attributable to the significance of SAH hydrodynamic performance, as **Figure 3b** expresses, the friction factor is also appraised for the comparison; the modified Blasius friction factor correlation for smooth ducts (Pritchard, P.J., Fox, R.W. and McDonald 2010) is applied, defined as:

$$f_s = 0.085Re^{-0.25} \quad (15)$$

A less than 7 % average error is observable in this figure. For further comparison, the experimental data of Priyam and Chand (2019) is reproduced in the current study for the thermal efficiency, illustrated in in **Figure 3c**. The disparity is about 7.5 %, on average. The comparisons are put forward to corroborate the present numerical procedure in apprehending the physics of the studied SAH.

The meshing process was performed using hexahedron 3D cells through a semi-organized method, by setting spatial zones. The quality functions, such as skewness, orthogonal quality, and aspect ratio, were also checked up. The near walls region was meshed by some layers of inflation to make sure about the low values of y+.

The grid independency from the solving procedure has to be implemented beforehand the numerical simulation. This is carried out for every case differing in boundary conditions and also geometrical characteristics, through the comparison of average Nusselt number and friction factor for various grid sizes. The appropriate cell numbers, after applying the grid independency test, are lower than 2 million cells for all cases. The procedure is shown in **Table 2**, as an instance. One can consider the cell numbers of 1,848,498, as the most affordable and precise mesh, according to the information in this table.

3. Results and discussion

In this section, the thermal and hydraulic results of the current numerical simulation for the SAH, inaugurated with fins for various amplitudes are presented. The results are ordered such that the performance of the introduced patterns is well understood. Firstly, the contours are demonstrated for the qualitative demonstration of the results and thereafter, several quantitative figures are presented.

Figure 4 reveals the dynamics of the flow pattern moving on the absorber by showing the streamlines. The figure indicates the fluid flow passage through the harmonic conduits that make the flow particles to be more in contact with the absorber and fins. This leads to higher heat transfer, as well as friction, which is delineated in the following. The streamlines trajectories are higher at larger Reynolds numbers, as expected. Further, the figures show that it takes a while after entering whereby the flow can coordinate and conform to the fins patterns. The wavy pattern makes the fluid flow more uniform than the raccoon pattern, which leads to a periodic contraction and expansion in the flow passage.

Figure 5 shows the temperature contour on the absorber plate. An efficient SAH makes a more uniform temperature distribution on the absorber plate and diminishes the high temperature on the plate. Case 1, which is a simple SAH, has not specified such an acceptable performance, qualitatively. Although the temperature decreases along the plate by passing of the fluid flow, most of the area of the absorber is kept at a high temperature, contrary to the high standards of capturing the best efficiency in photovoltaic SAHs. The maximum temperature of the absorber falls by increasing Reynolds number in case 1, similar to other cases. However, it requires more pumping energy that leads to the process being more expensive. Cases 2 and 5 maintain the absorber plate in a lower maximum temperature and more uniform distribution compared to the other cases. Cases

3 and 4 also present the maximum temperature near the values found in cases 2 and 5. Increasing Reynolds number elicits a reduction in maximum temperature; approximately 4 % (for case 1) and 1-2 % (for other cases). The results reveal that no considerable difference is found between the cases of wavy and raccoon configurations in terms of absorber plate temperature.

Figure 6 shows the turbulent kinetic energy (TKE) of the fluid flow on the absorber, in a similar arrangement to **Figure 5**. TKE is crucial to strengthen the mixing of the core flow and the layer attached to the absorber plate. The lower minimum value belongs to case 1, which shows no improvement even by increasing the Reynolds number. The sinusoidal paths on the other cases play a fundamental role in intensifying turbulence level on the absorber; among them, cases 2 and 4 illustrate a higher value of TKE, more than 150 to 300 % in $Re = 12000$, in comparison to the other finned cases. These cases indicate that the core region of the channel flow extra contributes to TKE production, which underscores the importance of fins' amplitude in rising turbulence level, resulting in higher mixing and more boundary layers devouring. Although the hydraulic performance of these cases should be evaluated, cases 2 and 4 are expected to have reasonable thermal performance. The effect of the Reynolds number on TKE of all studied cases is thermally aggravating; cases 2 and 4 show the most drastic improvement. The latter makes more than 4 times increment in TKE, while maximum 2.5-fold rising is found in other cases by raising the Reynolds number. Wavy configuration denotes a slightly better response, having higher and identical TKE distribution on the absorber.

Figure 7 presents the temperature at the outlet of the SAH, as the output of the solar heating process for electrical or thermal applications. The uniform distribution temperature at the outlet is advantageous and can diminish the standard deviation and leads to the average temperature as the acceptable representative of the heated airflow for thermodynamic calculations. The non-uniform

thermal airflow at the outlet, on the other hand, is considered a poor outcome, which limits SAH application. Outlet airflow of case 1 has the highest temperature among all the studied cases. This belongs to the layer in the vicinity of the absorber plate, while the bottom plate experiences the temperature of the inlet flow field. This shows that the affected zone of the SAH of case 1 is restricted to those near the hot plate, and the mixing between thermally different zones is too weak. This makes solar heat transfer to be inefficient with a high gradient. The maximum temperature and thermal gradient are subsided through the outlet in finned cases, especially in cases 2 and 5, representing a sufficient thermal performance. Nonetheless, the higher temperature zone is still found near the absorber plate. Increasing Reynolds number mitigates steep gradients by increasing the convective heat transfer coefficient.

The Mean Nusselt number is demonstrated in **Figure 8** for various cases investigated. In support of the earlier results demonstrated, case 2 obtains the maximum value of the Nusselt number. It shows a value of about 3 times higher than case 1. Case 4 is followed with a high value of the Nusselt number and afterward, cases 3 and 5 are arranged. The Nusselt number in cases 2 and 4 are about 14 % larger than those in cases 3 and 5, on average for Re=12000. The preceding difference reaches 20 % by increasing the Reynolds number, as this enhances heat transfer. This indicates the crucial effects of fins' amplitude on the Nusselt number. The heat transfer can, therefore, enhance considerably if the amplitude rises two-fold. This addresses a simple, easy, and inexpensive geometrical change which leads to a useful thermal advancement. The Nusselt number upraises about 80 % by increasing Reynolds number, on average. Further, the highest value of the Nusselt number obtains the value 7 times greater than the lowest. The results conspicuously prove the thermal benefits of enlarging the fins' amplitude. No conclusion is derived from the preference of wavy or raccoon configuration by consideration of Nusselt number.

The friction factor is a criterion to assess the hydraulic performance and energy consumption of many thermal systems, such as SAHs. The best thermal cases are stemmed from the most frictional cases. Case 2 and 4 present a 70 % higher friction factor than those of cases 3 and 5, on average, as observed in **Figure 9**, which is considerable. Despite the thermal advantages of the fins' amplitude increment, this features a higher cost for flow pumping. However, it cannot lead to a conclusion, before both thermal and hydrodynamic evaluations are set together, as the next figure shows. Case 1, which comprises the poorest thermal response, shows the lowest hydraulic loss by a friction factor of 0.01. Interestingly, the Reynolds number has no considerable effect on the friction factor. In cases with fins, case 3 has the lowest value of friction factor.

For investigations on the hydraulic loss of the proposed configurations, **Table 3** tabulates the pressure drop and power demand for the cases studied. It reveals that case 1 still needs the lowest value of power in comparison to the other cases. Similar to what is observed in **Figure 9**, cases 2 and 4 consume the highest value of power, if they are installed. The highest values approach about 12 and 16 times what is required for case 1, respectively for Re=12000 and 24000. However, the absolute values for power demand show little current costs for the introduced solar air heater with fins, if it is evaluated by the power demand of a normal electrical lampshade. Increasing Reynolds number can increase the electricity payment bill by a factor of 7-8. The variations of pressure drop are also similar to what was described for power demand, noted above.

Thermo-hydraulic performance factor ($THPF$) is an index for thermal-hydraulic evaluability of thermal systems and the SAH follows suit; this index is presented here for the current finned patterns for cases 2 to 5 in **Figure 10**. At $Re = 12000$, case 3 ($THPF = 1.75$) and at $Re = 24000$, case 2 ($THPF = 2.15$) illustrates the best performance. Despite heat transfer as well as friction factor increment, shown in **Figure 8** and **Figure 9**, the current figure can prove the ability to

increase fins' amplitude to thermo-hydrodynamically upgrade a solar air heater, as the highest value of $THPF$ is achieved in case 2. However, it indicates that the upgrade can be occurred only in special conditions; here it is given at Re=24000. The minimum value of $THPF$ belongs to case 4 for the two Reynolds numbers investigated. $THPF$ can be improved more than 15 % by increasing Reynolds number, averagely. This figure shows that the wavy configuration can lead to higher thermo-hydraulic performance than raccoon fins, by approximately 10 %. The absolute values of $THPF$ for cases studied show acceptable performance in terms of energy management.

The $THPF$ is compared between the current results and that in Refs. (Chokphoemphun et al. 2015) and (Antony et al. 2020), in which the SAH performance is upgraded using turbulators attached beneath the absorber plate. **Figure 11** shows this comparison. This demonstrates that $THPF$ in the current study grows more than 50 and 110 % respectively for $Re = 12000$ and 24000, indicates that the current study takes a tangible step in the literature to improve not only heat transfer, but also thermo-hydraulic performance and, can be considered as an applicable idea.

4. Conclusion

The current work simulated a solar air heater characterized by wavy and raccoon fin patterns and two different amplitudes. The temperature contours, outlet and Nusselt number on the absorber plate, friction factor, and thermo-hydraulic performance of the fluid flow were assessed. The concluding remarks are outlined herein:

- The maximum temperature on the absorber was mitigated as the Reynolds number increased. This decreased the maximum temperature by about 4 percent for simple channel and 1-2 percent for the finned configurations.

- Higher amplitude of sinusoidal fins kept the absorber plate in a lower maximum temperature and more uniform distribution, while wavy and raccoon configurations resulted in no difference in the absorber temperature.
- The sinusoidal paths on the finned cases made a fundamental role for intensifying turbulence level on the absorber. The case with higher amplitude could illustrate a higher value of turbulent kinetic energy more than 150 to 300 percent in comparison to the other finned cases.
- The maximum temperature and thermal gradient were subsided through the outlet by using the fins in the solar air heater. The case with the highest amplitude and wavy configuration specified the maximum value of the Nusselt number by about 3 times higher value than the simple case. On average, the Nusselt number upraised about 80 percent by increasing the Reynolds number.
- The Reynolds number had no considerable effect on the friction factor.
- Thermal performance factor improved more than 15 percent on average by increasing Reynolds number. The wavy configuration indicated higher thermo-hydraulic performance than that of raccoon fins, by about 10 percent.
- The proposed configurations could increase the thermal performance factor in comparison with the earlier studies.

5. Data Availability

The data produced in this study can be obtained by direct email to the corresponding author.

6. References

Antony AL, Shetty SP, Madhwesh N, Yagnesh Sharma N, Vasudeva Karanth K. 2020. Influence

of stepped cylindrical turbulence generators on the thermal enhancement factor of a flat plate solar air heater. Sol Energy. 198:295–310. doi:10.1016/j.solener.2020.01.065.

Arul Kumar R, Ganesh Babu B, Mohanraj M. 2016. Thermodynamic performance of forced convection solar air heaters using pin–fin absorber plate packed with latent heat storage materials. J Therm Anal Calorim 2016 1263. 126(3):1657–1678. doi:10.1007/S10973-016-5665-6. [accessed 2021 Aug 11]. https://link.springer.com/article/10.1007/s10973-016-5665-6.

Arunkumar HS, Vasudeva Karanth K, Kumar S. 2020. Review on the design modifications of a solar air heater for improvement in the thermal performance. Sustain Energy Technol Assessments. 39:100685. doi:10.1016/j.seta.2020.100685.

Boulemtafes-Boukadoum A, Benzaoui A. 2014. CFD based Analysis of Heat Transfer Enhancement in Solar Air Heater Provided with Transverse Rectangular Ribs. Energy Procedia. 50:761–772. doi:10.1016/j.egypro.2014.06.094. https://doi.org/10.1016%2Fj.egypro.2014.06.094.

Chokphoemphun S, Pimsarn M, Thianpong C, Promvonge P. 2015. Thermal performance of tubular heat exchanger with multiple twisted-tape inserts. Chinese J Chem Eng. 23(5):755–762. doi:10.1016/j.cjche.2015.01.003.

ElGamal R, Kishk S, Al-Rejaie S, ElMasry G. 2020 Nov. Incorporation of a solar tracking system for enhancing the performance of solar air heaters in drying apple slices. Renew Energy. doi:10.1016/j.renene.2020.11.137. https://doi.org/10.1016%2Fj.renene.2020.11.137.

Gawande VB, Dhoble AS, Zodpe DB, Chamoli S. 2016. A review of CFD methodology used in literature for predicting thermo-hydraulic performance of a roughened solar air heater. Renew Sustain Energy Rev. 54:550–605. doi:10.1016/j.rser.2015.10.025. https://doi.org/10.1016%2Fj.rser.2015.10.025.

Hu H, Li J. 2021. Experimental investigation on heat transfer characteristics of two-phase flow boiling in offset strip fin channels of plate-fin heat exchangers. Appl Therm Eng. 185:116404. doi:10.1016/j.applthermaleng.2020.116404.
https://doi.org/10.1016%2Fj.applthermaleng.2020.116404.

Issacci F, Zvirin Y, Grossman G. 1988. Heat transfer analysis of a finned solar air heater. J Sol Energy Eng Trans ASME. 110(2):145–155. doi:10.1115/1.3268245.

Kannan C, Mohanraj M, Sathyabalan P. 2020. Experimental investigations on jet impingement solar air collectors using pin-fin absorber. Proc Inst Mech Eng Part E J Process Mech Eng. 235(1):134–146. doi:10.1177/0954408920935301. https://doi.org/10.1177/0954408920935301.

Kasperski J, Nemś M. 2013. Investigation of thermo-hydraulic performance of concentrated solar air-heater with internal multiple-fin array. Appl Therm Eng. 58(1–2):411–419. doi:10.1016/j.applthermaleng.2013.04.018.

Kumar A, Layek A. 2019. Nusselt number and friction factor correlation of solar air heater having twisted-rib roughness on absorber plate. Renew Energy. 130:687–699. doi:10.1016/j.renene.2018.06.076.

Kumar R, Chand P. 2017. Performance enhancement of solar air heater using herringbone corrugated fins. Energy. 127:271–279. doi:10.1016/j.energy.2017.03.128.

Kumar R, Goel V, Bhattacharyya S, Tyagi V V, Abusorrah AM. 2021 Apr 25. Experimental investigation for heat and flow characteristics of solar air heater having symmetrical gaps in multiple-arc rib pattern as roughness elements. Exp Heat Transf.:1–18. doi:10.1080/08916152.2021.1905752. https://doi.org/10.1080/08916152.2021.1905752.

Kumar R, Goel V, Kumar M. 2020. Effect of providing gap in multiple-arc rib-roughened solar air heater - Part 1. J Mech Sci Technol. 34(6):2619–2625. doi:10.1007/s12206-020-0535-3. https://doi.org/10.1007/s12206-020-0535-3.

Kumar R, Goel V, Singh P, Saxena A, Kashyap AS, Rai A. 2019. Performance evaluation and optimization of solar assisted air heater with discrete multiple arc shaped ribs. J Energy Storage. 26:100978. doi:https://doi.org/10.1016/j.est.2019.100978. https://www.sciencedirect.com/science/article/pii/S2352152X19304657.

Kumar R, Kashyap AS, Singh P, Goel V, Kumar K. 2020. Innovatively Arranged Curved-Ribbed Solar-Assisted Air Heater: Performance and Correlation Development for Heat and Flow Characteristics. J Sol Energy Eng. 142(3). doi:10.1115/1.4045827.

Kumar R, Kumar A, Goel V. 2017. A parametric analysis of rectangular rib roughened triangular duct solar air heater using computational fluid dynamics. Sol Energy. 157:1095–1107. doi:10.1016/j.solener.2017.08.071. https://doi.org/10.1016%2Fj.solener.2017.08.071.

Madhlopa A, Jones SA, Saka JDK. 2002. A solar air heater with composite-absorber systems for food dehydration. Renew Energy. 27(1):27–37. doi:10.1016/s0960-1481(01)00174-4. https://doi.org/10.1016%2Fs0960-1481%2801%2900174-4.

Madhu B, Kabeel AE, Sathyamurthy R, Sharshir SW, Manokar AM, Raghavendran PR, Chandrashekar T, Mageshbabu D. 2020. Investigation on heat transfer enhancement of conventional and staggered fin solar air heater coated with CNT-black paint—an experimental approach. Environ Sci Pollut Res. 27(26):32251–32269. doi:10.1007/s11356-019-07561-1. [accessed 2020 Nov 30]. https://link.springer.com/article/10.1007/s11356-019-07561-1.

Naphon P. 2005. On the performance and entropy generation of the double-pass solar air heater with longitudinal fins. Renew Energy. 30(9):1345–1357. doi:10.1016/j.renene.2004.10.014.

Paraschiv S, Bărbuţă-Mişu N, Paraschiv LS. 2020. Technical and economic analysis of a solar air heating system integration in a residential building wall to increase energy efficiency by solar heat gain and thermal insulation. Energy Reports. 6:459–474. doi:10.1016/j.egyr.2020.09.024. https://doi.org/10.1016%2Fj.egyr.2020.09.024.

Pritchard, P.J., Fox, R.W. and McDonald AT. 2010. Introduction to fluid mechanics. John Wiley & Sons, Ltd.

Priyam A, Chand P. 2016. Thermal and thermohydraulic performance of wavy finned absorber solar air heater. Sol Energy. 130:250–259.

Priyam A, Chand P. 2017. Heat transfer and pressure drop characteristics of wavy fin solar air heater. Int J Heat Technol. 35(4):1015–1022. doi:10.18280/ijht.350438. [accessed 2020 Nov 30]. http://www.iieta.org/sites/default/files/Journals/IJHT/35.04_38.pdf.

Priyam A, Chand P. 2018. Thermal performance of wavy finned absorber solar air heater. Int J Heat Technol. 36(4):1393–1403. doi:10.18280/ijht.360431. [accessed 2020 Nov 30].

http://www.iieta.org/journals/ijht/paper/10.18280/ijht.360431.

Priyam A, Chand P. 2019. Experimental investigations on thermal performance of solar air heater with wavy fin absorbers. Heat Mass Transf. 55(9):2651–2666. doi:10.1007/s00231-019-02605-1. [accessed 2020 Nov 29]. https://link.springer.com/article/10.1007/s00231-019-02605-1.

Qader BS, Supeni EE, Ariffin MKA, Talib ARA. 2019. Numerical investigation of flow through inclined fins under the absorber plate of solar air heater. Renew Energy. 141:468–481. doi:10.1016/j.renene.2019.04.024.

Raj AK, Srinivas M, Jayaraj S. 2019. A cost-effective method to improve the performance of solar air heaters using discrete macro-encapsulated PCM capsules for drying applications. Appl Therm Eng. 146:910–920. doi:10.1016/j.applthermaleng.2018.10.055. https://doi.org/10.1016%2Fj.applthermaleng.2018.10.055.

Sadeghianjahromi A, Wang C-C. 2020 Oct. Heat transfer enhancement in fin-and-tube heat exchangers - A review on different mechanisms. Renew Sustain Energy Rev.:110470. doi:10.1016/j.rser.2020.110470. https://doi.org/10.1016%2Fj.rser.2020.110470.

Sahu MK, Sharma M, Matheswaran MM, Maitra K. 2019. On the Use of Longitudinal Fins to Enhance the Performance in Rectangular Duct of Solar Air Heaters - A Review. J Sol Energy Eng Trans ASME. 141(3). doi:10.1115/1.4042827.

Sertkaya AA, Sari S. 2021. Experimental Investigation of Heat Transfer Depending on Inclination Angle of Unfinned, Axial Finned and Radial Finned Heat Exchangers. Int J Heat Mass Transf. 165:120704. doi:10.1016/j.ijheatmasstransfer.2020.120704. https://doi.org/10.1016%2Fj.ijheatmasstransfer.2020.120704.

Singh AP, Varun, Siddhartha. 2014a. Effect of artificial roughness on heat transfer and friction characteristics having multiple arc shaped roughness element on the absorber plate. Sol Energy. 105:479–493. doi:https://doi.org/10.1016/j.solener.2014.04.007. https://www.sciencedirect.com/science/article/pii/S0038092X14001923.

Singh AP, Varun, Siddhartha. 2014b. Heat transfer and friction factor correlations for multiple arc shape roughness elements on the absorber plate used in solar air heaters. Exp Therm Fluid Sci. 54:117–126. doi:https://doi.org/10.1016/j.expthermflusci.2014.02.004. https://www.sciencedirect.com/science/article/pii/S089417771400034X.

Singh I, Singh S. 2018. CFD analysis of solar air heater duct having square wave profiled transverse ribs as roughness elements. Sol Energy. 162:442–453. doi:10.1016/j.solener.2018.01.019.

Singh S. 2020. Experimental and numerical investigations of a single and double pass porous serpentine wavy wiremesh packed bed solar air heater. Renew Energy. 145:1361–1387. doi:10.1016/j.renene.2019.06.137.

Singh S, Anand A, Shukla A, Sharma A. 2020. Technical, financial, and environmental feasibility of solar water heater for residential, commercial, and industrial application: A theoretical approach. Mater Sci Energy Technol. 3:648–671. doi:10.1016/j.mset.2020.07.001. https://doi.org/10.1016%2Fj.mset.2020.07.001.

Sivakumar S, Siva K, Mohanraj M. 2019. Experimental thermodynamic analysis of a forced

convection solar air heater using absorber plate with pin-fins. J Therm Anal Calorim. 136(1):39–47. doi:10.1007/s10973-018-07998-5. https://doi.org/10.1007/s10973-018-07998-5.

Skullong S, Promthaisong P, Promvonge P, Thianpong C, Pimsarn M. 2018. Thermal performance in solar air heater with perforated-winglet-type vortex generator. Sol Energy. 170:1101–1117. doi:https://doi.org/10.1016/j.solener.2018.05.093. https://www.sciencedirect.com/science/article/pii/S0038092X18305358.

Skullong S, Promvonge P, Thianpong C, Pimsarn M. 2016. Thermal performance in solar air heater channel with combined wavy-groove and perforated-delta wing vortex generators. Appl Therm Eng. 100:611–620. doi:10.1016/j.applthermaleng.2016.01.107.

Speziale CG, Thangam S. 1992. Analysis of an RNG based turbulence model for separated flows. Int J Eng Sci. 30(10):1379-IN4. doi:https://doi.org/10.1016/0020-7225(92)90148-A. https://www.sciencedirect.com/science/article/pii/002072259290148A.

Szablewski W. 1973. B. E. Launder and D. B. Spalding, Mathematical Models of Turbulence. 169 S. m. Abb. London/New York 1972. Academic Press. Preis geb. ZAMM - Zeitschrift für Angew Math und Mech. 53(6):424–424. doi:10.1002/zamm.19730530619. [accessed 2020 Dec 21]. http://doi.wiley.com/10.1002/zamm.19730530619.

Theodore L. Bergman ASLFPIDPD. 2011. Fundamentals of Heat and Mass Transfer, 8th Edition | Wiley. Wiley.

Treichel C, Cruickshank CA. 2021. Economic analysis of heat pump water heaters coupled with air-based solar thermal collectors in Canada and the United States. J Build Eng. 35:102034. doi:10.1016/j.jobe.2020.102034. https://doi.org/10.1016%2Fj.jobe.2020.102034.

Xue Y, Ge Z, Du X, Yang L. 2018. On the Heat Transfer Enhancement of Plate Fin Heat Exchanger. Energies. 11(6). doi:10.3390/en11061398. https://www.mdpi.com/1996-1073/11/6/1398.

Yadav AS, Bhagoria JL. 2013a. Heat transfer and fluid flow analysis of solar air heater: A review of CFD approach. Renew Sustain Energy Rev. 23:60–79. doi:10.1016/j.rser.2013.02.035. https://doi.org/10.1016%2Fj.rser.2013.02.035.

Yadav AS, Bhagoria JL. 2013b. Modeling and Simulation of Turbulent Flows through a Solar Air Heater Having Square-Sectioned Transverse Rib Roughness on the Absorber Plate. Sci World J. 2013:1–12. doi:10.1155/2013/827131. https://doi.org/10.1155%2F2013%2F827131.

Yadav S, Saini RP. 2020. Numerical investigation on the performance of a solar air heater using jet impingement with absorber plate. Sol Energy. 208:236–248. doi:10.1016/j.solener.2020.07.088.

Yakhot V, Orszag SA, Thangam S, Gatski TB, Speziale CG. 1992. Development of turbulence models for shear flows by a double expansion technique. Phys Fluids A Fluid Dyn. 4(7):1510–1520. doi:10.1063/1.858424. https://doi.org/10.1063/1.858424.

Table 1. Studied cases in this work.

Case No.	Absorber's fin type	Waviness ($\gamma = A/\lambda$)
1	Without fin (Base model)	-
2	Wavy	0.167
3	Wavy	0.084
4	Raccoon	0.167
5	Raccoon	0.084

Table 2. Grid independency procedure.

Cell numbers	Average Nusselt number	Relative Error (%)
683,294	172.11	-
1,076,548	199.68	16.01883
1,848,498	221.96	11.15785
2,668,677	223.33	0.617228

Table 3. The pressure drop and power demand.

Case No.	$Re = 12000$		$Re = 24000$	
	Pressure drop (pa)	Power (w)	Pressure drop (pa)	Power (w)
1	9.41	0.17	26.35	0.93
2	112.30	1.98	430.11	15.14
3	42.88	0.75	160.8	5.66
4	118	2.08	470.40	16.56
5	51	0.90	196.3	6.91

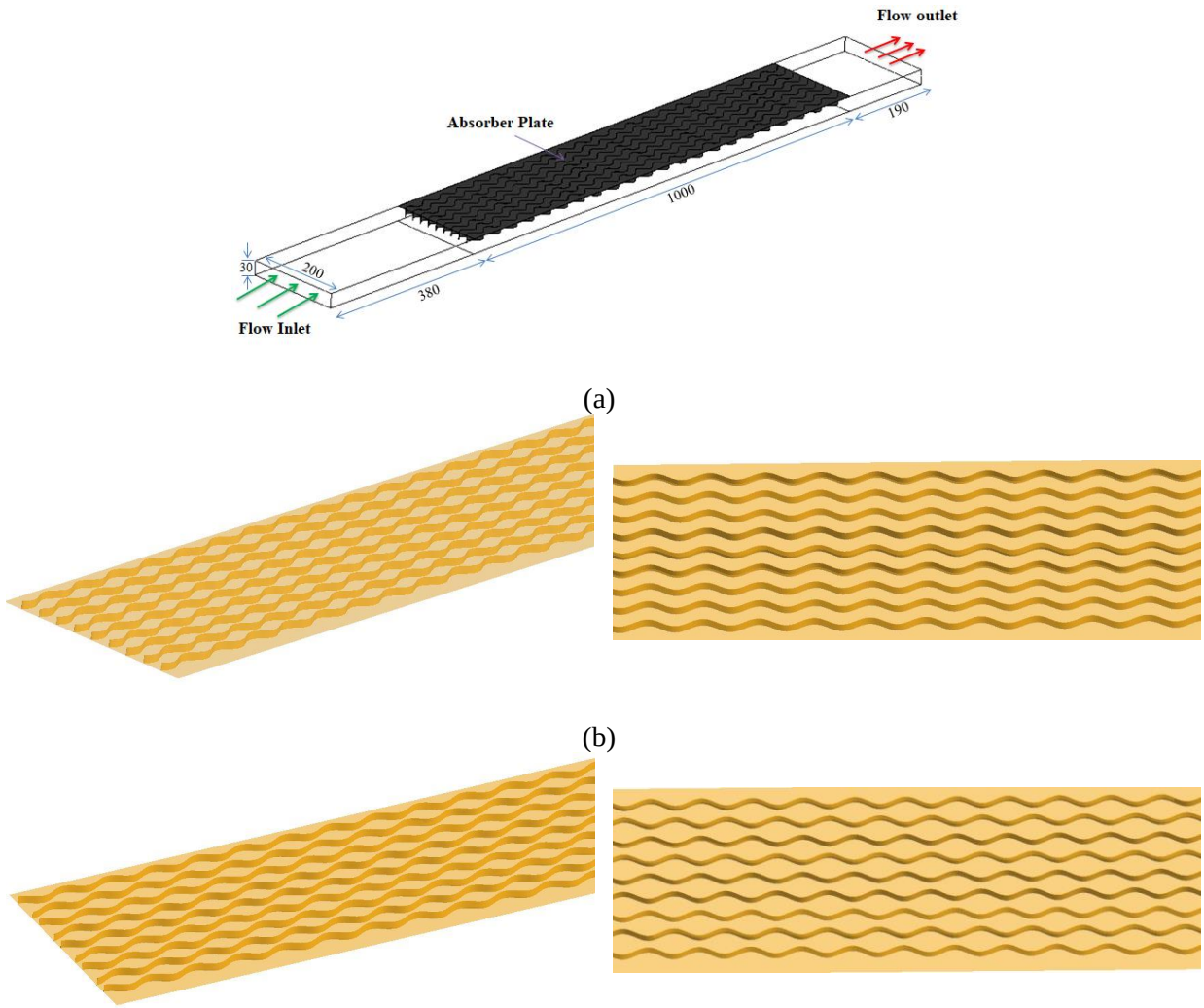

Figure 1. (a) The geometry of the SAH with fins on the absorber plate, (b) the wavy, and (c) the raccoon configuration.

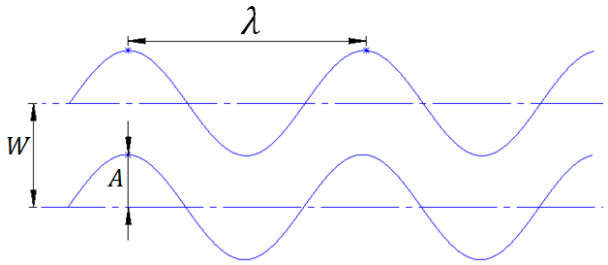

Figure 2. The fin's geometry specification.

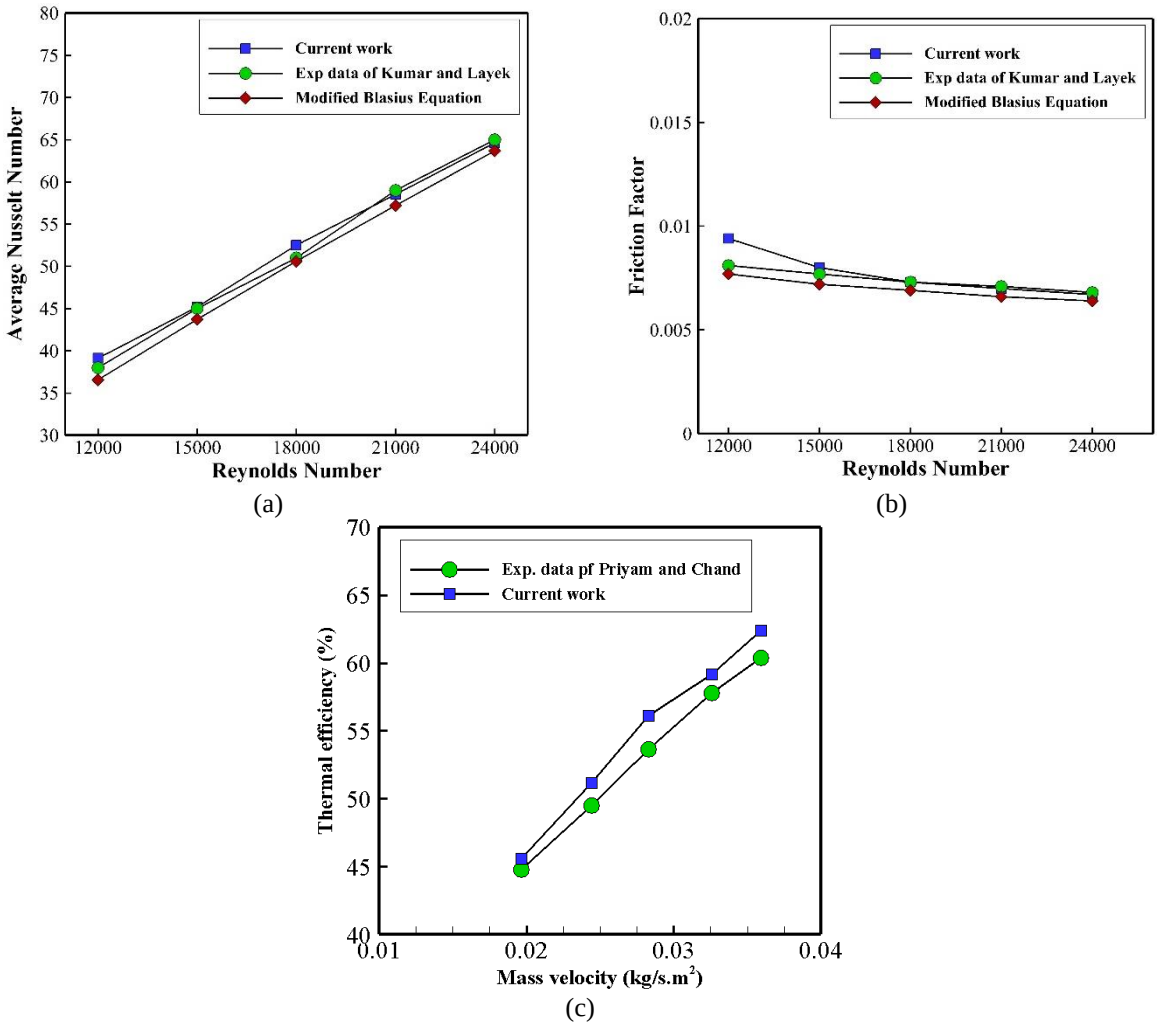

Figure 3. The comparison between the current results and those published earlier for (a) the average Nusselt number, (b) the friction factor comparison versus Reynolds number, and (c) the thermal efficiency versus mass velocity: the validation process.

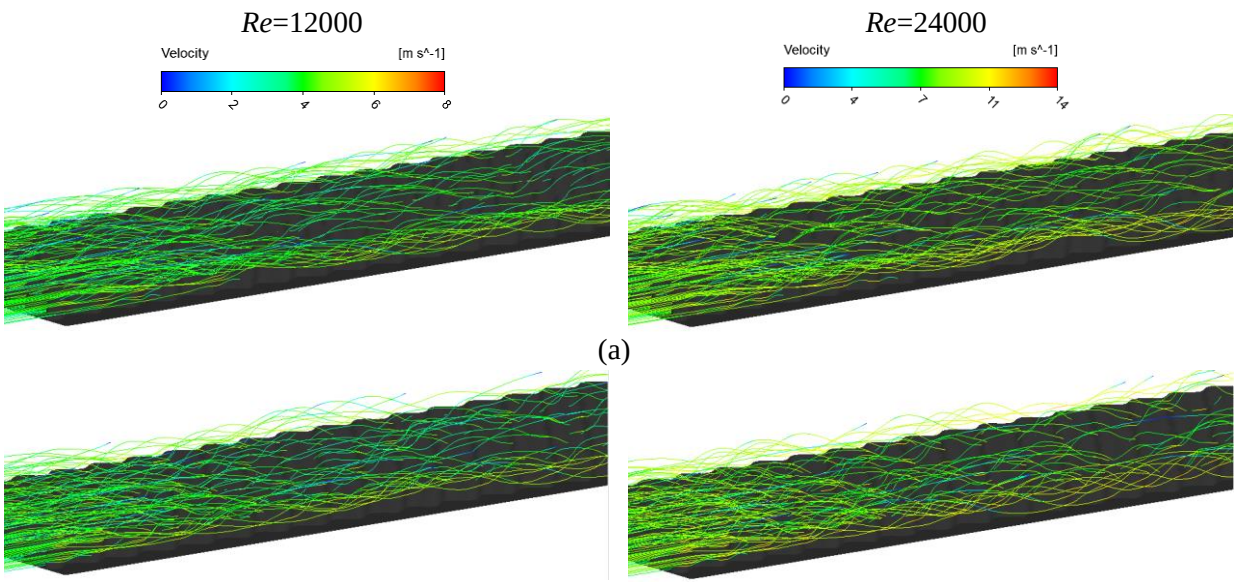

(a)

(b)

Figure 4. The streamlines pattern on the absorber plate for $Re = 12000$ and $Re = 24000$ at (a) case 2 and (b) case 4.

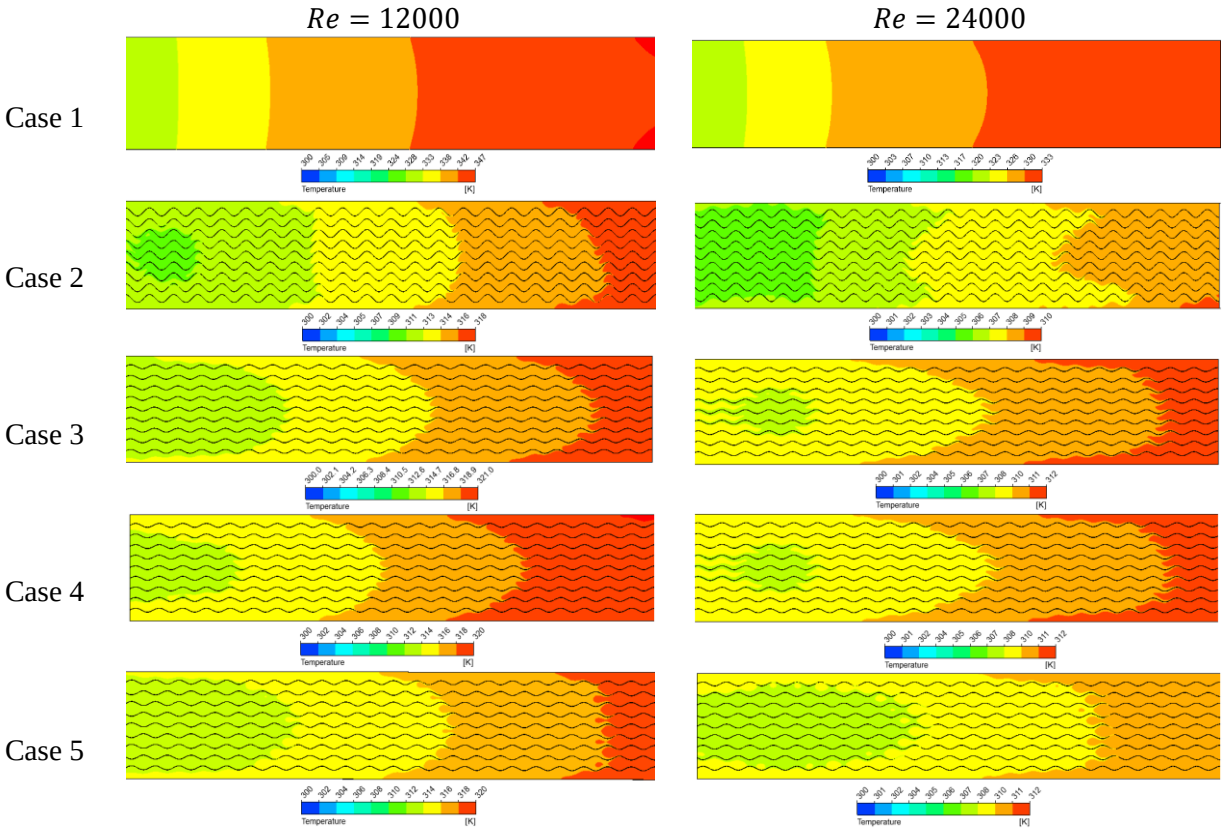

Figure 5. The temperature contour on the absorber plates of various cases in $Re = 12000$ and 24000.

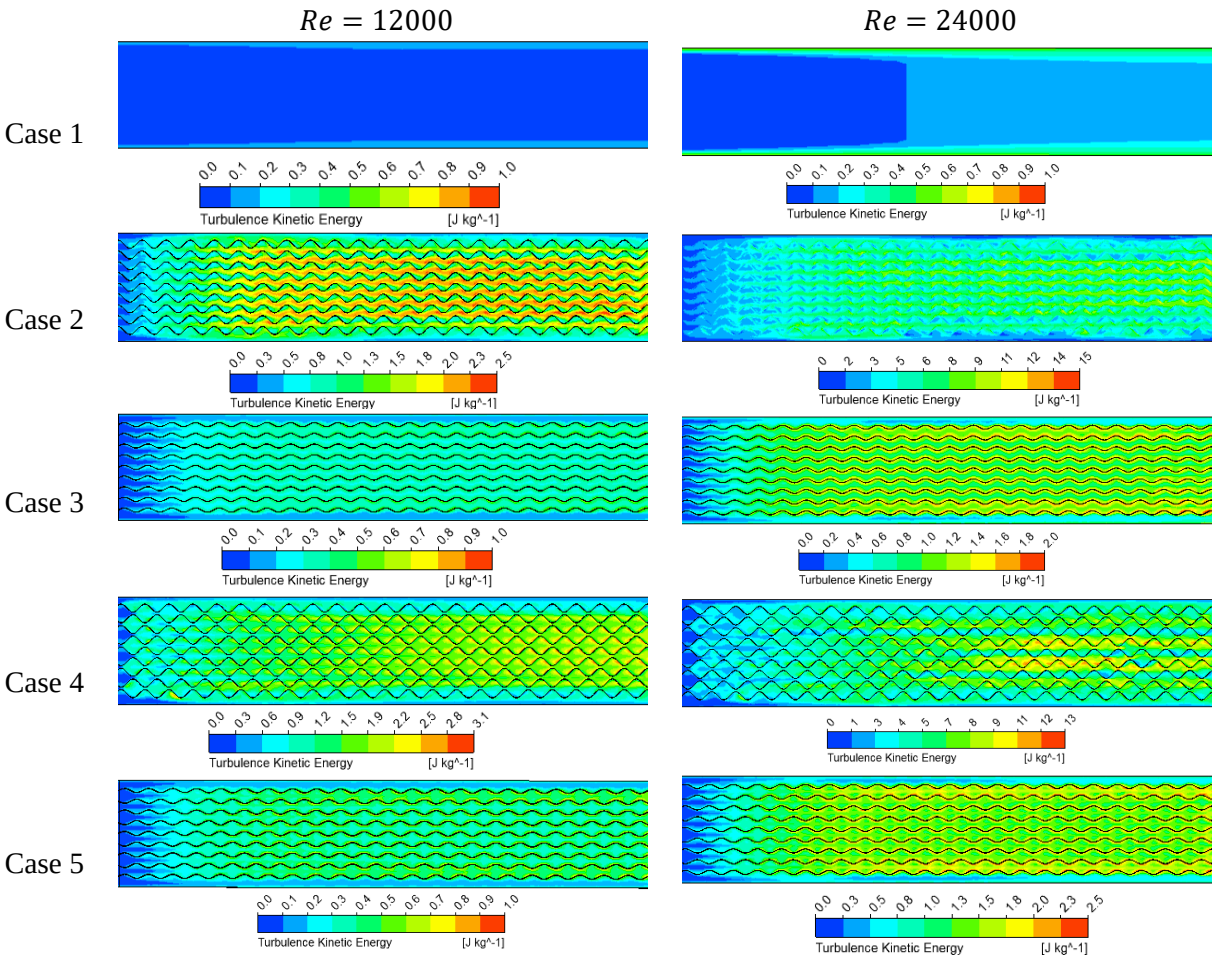

Figure 6. Turbulent kinetic energy contour on the absorber plate for various cases in $Re = 12000$ and 24000.

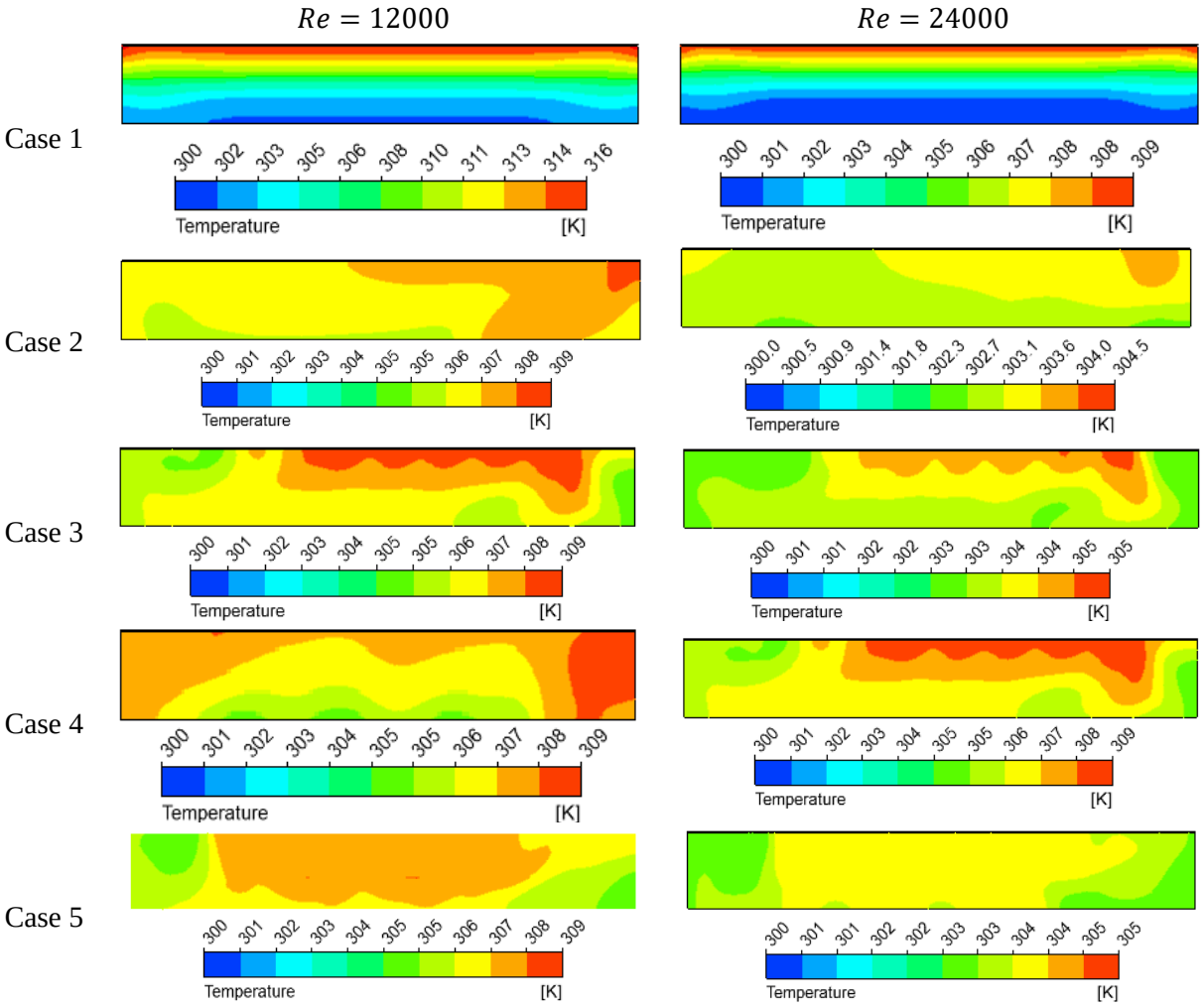

Figure 7. Temperature contour on the outlet for various cases in $Re = 12000$ and 24000.

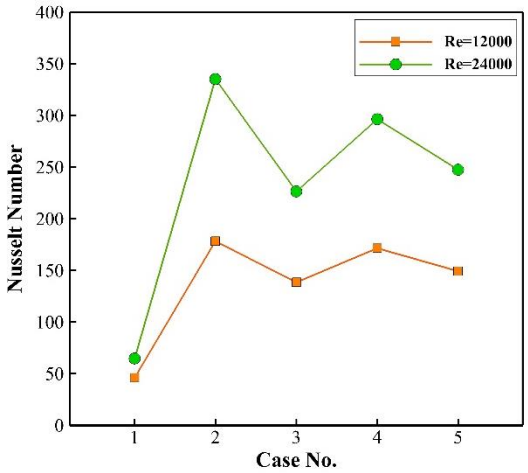

Figure 8. Mean Nusselt number on the absorber plate for cases 1 to 5 and $Re = 12000$ and 24000.

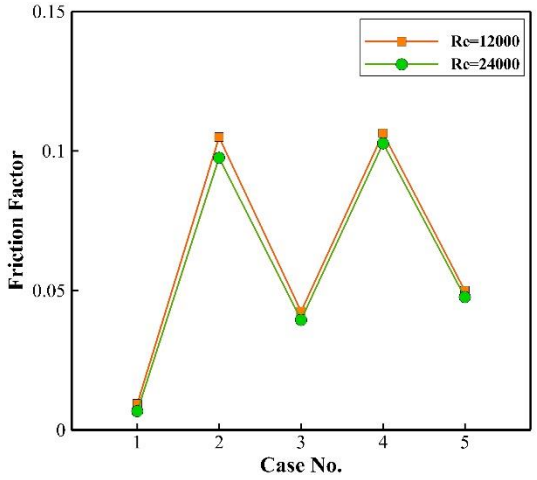

Figure 9. The friction factor of the fluid flow for cases 1 to 5 and $Re = 12000$ and 24000.

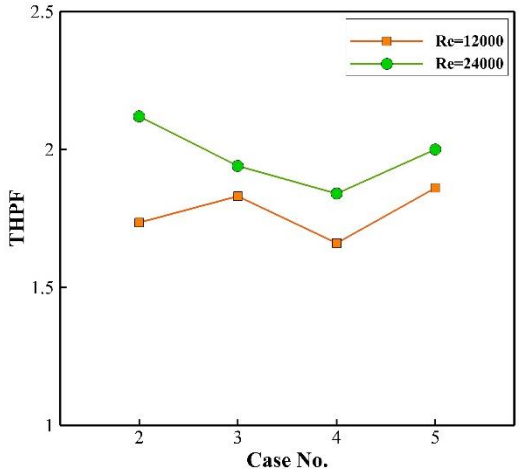

Figure 10. The thermo-hydraulic performance factor of the fluid flow for cases 2 to 5 and $Re = 12000$ and 24000

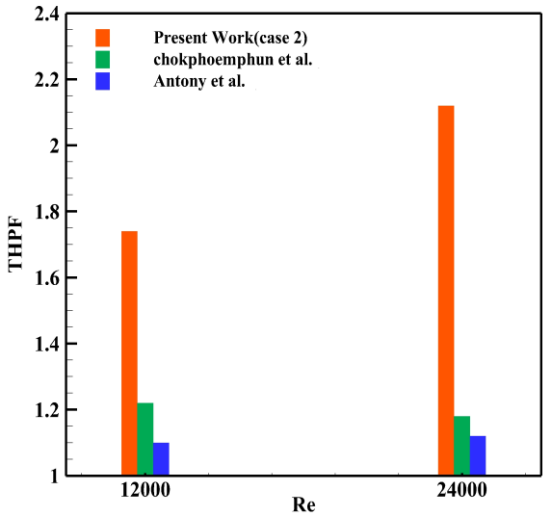

Figure 11. A comparison of thermal performance factor between the current results and the similar works of Refs. (Chokphoemphun et al. 2015) and (Antony et al. 2020)